Universitat Autònoma de Barcelona

Dipòsit digital de documents de la UAB

This is the **accepted version** of the article:

Robbennolt, Shauna; Fornell Beringues, Jordina; Quintana Romero, Alberto; [et al.]. «Structural and magnetic properties of FexCu1-x sputtered thin films electrochemically treated to create nanoporosity for high-surface-area magnetic components». ACS Applied Nano Materials, Vol. 1, Issue 4 (April 2018), p. 1675-1682. DOI 10.1021/acsanm.8b00143

This version is available at https://ddd.uab.cat/record/233391

under the terms of the IN COPYRIGHT license

Structural and Magnetic Properties of FexCu1−x Sputtered Thin Films Electrochemically Treated To Create Nanoporosity for High-SurfaceArea Magnetic Components

Shauna Robbennolt,*,† Jordina Fornell,† Alberto Quintana,† Huiyan Zhang,† Enric Menendez,† Eva Pellicer,*,† and Jordi Sort*,†,‡

† Departament de Física, Universitat Autonoma de Barcelona, E-08193 Bellaterra, Spain

‡ InstitucióCatalana de Recerca i Estudis Avancats (ICREA), Pg. Lluís Companys 23, E-08010 Barcelona, Spain

ABSTRACT: Sputter deposition is a facile and widely used technique for fabricating thin-film materials. Electrochemical dealloying, on the other hand, is a promising method for creating nanoporosity, and therefore increasing surface area, in metallic materials. Surprisingly, little work has been done on the application of electrochemical dealloying to sputterdeposited thin films. Here, we prepare FexCu1−x thin films by sputter deposition to be then electrochemically treated to create porosity. We investigate the structural and magnetic properties of as-sputtered and electrochemically treated films. We find that the morphology, crystal structure, and magnetic properties are highly dependent on initial film composition. For high copper content films (Fe29Cu71), relative Cu content is found to decrease during the dealloying process. For these films, the crystal structure is not greatly affected by the induced porosity and the porous films show increased saturation magnetization. However, for the more Fe-rich compositions (Fe63Cu37), we find that Fe is preferentially lost and making the films nanoporous induces a crystal structure change from body-centered cubic (bcc) to a mixture of face-centered cubic (fcc) and bccphases. These same porous films show a decrease in saturation magnetization and a large increase in coercivity compared to the as-sputtered films. These films are attractive as high-surface-area magnetic components because of the tunability of their magnetic properties and their high surface area due to porosity. To the best of our knowledge, these results constitute the first example of nanoporous, magnetic thin films by prepared by sputtering and subsequent electrochemical treatment.

KEYWORDS: nanoporous, magnetron sputtering, FeCu, magnetic thin films, electrochemical dealloying

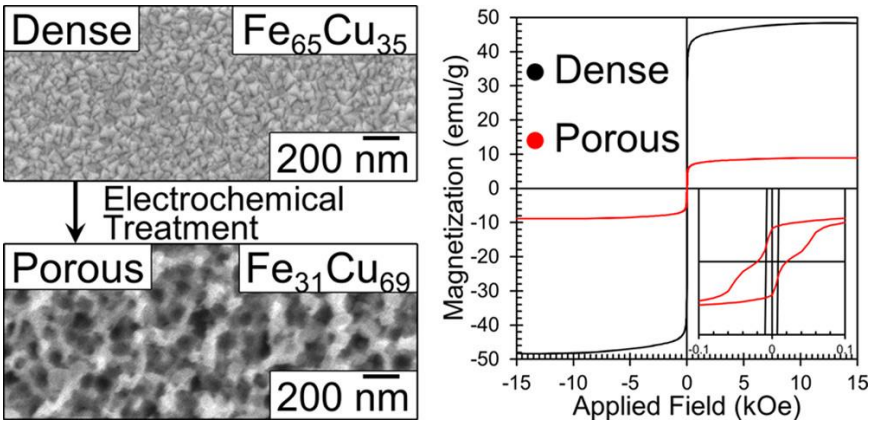

1. INTRODUCTION

Materials with 3D nanoporosity have attracted significant research interest. Because of their porosity, these materials have a large surface area, which is useful for applications ranging from catalysis1−9 to energy storage.2,4,10−13 In the case of catalysis, nanoporous magnetic materials are particularly attractive because they are magnetically recoverable. Despite the advantages of nanoporous materials, they are not currently widely used commercially, partly due to the limitations of current fabrication methods. A common method to prepare porous materials is to use a sacrificial templating agent such as polymers, surfactants (soft templating), porous silica, or anodic alumina (hard templating).7,14−20 In these cases, the material is grown in or around the template which is then removed, leaving pores in its place. Although effective in a research setting, these methods are not very scalable and often require reasonably expensive templates.

Among corrosion methods, electrochemical dealloying is a promising technique for fabricating nanoporous metals in a scalable manner without the need for a sacrificial template.3,21−25 Electrochemical dealloying is a method for forming a porous metal or metal alloy by selectively dissolving the most electrochemically active element in an alloy. It is important to note that this type of electrochemical dealloying is highly dependent on composition. If the fraction of the nobler element (i.e., the less electrochemically active element) is too high, above what is called the “parting limit”, both elements are then removed. On the other hand, if the fraction of the nobler element is too low, then as the dealloying progresses, there is insufficient noble element available for passivation, and the entire structure can dissolve or collapse.10,26 This technique has been used on bulk metals,21−24,26 ribbons,3 as well as thin films made by a variety of methods such as electrodeposition,27 electron beam deposition,28 and sputter deposition.29 Of particular interest is the application of electrochemical dealloying to create porosity in sputtered films. Sputtering is a highly effective and industrially scalable technique that is widely used to produce thin films. However, there are very few examples of porous films being made directly via sputtering alone.30,31 In some systems, porosity can be induced, but only to some extent and in a rather inhomogeneous manner, by tuning the Ar+ gas pressure in the sputtering chamber or the deposition angle during the growth of the films.30,31 Combining sputter deposition with electrochemical dealloying could therefore be a promising route to fabricate homogeneous porous thin films in a facile and reproducible way.

Here we have investigated the structural and magnetic properties of FexCu1−x (31 ≤ x ≤ 73, at %) thin films fabricated in this manner. FexCu1−x is an attractive material system to study both because it is magnetically soft and made from earthabundant elements making it useful in sustainable devices. In addition, previous theoretical studies have suggested that Cu can force the Fe into the face-centered cubic (fcc) structure, which can lead to a higher magnetic moment per Fe atom than in body-centered cubic (bcc)-Fe alone.32−34 We investigated the structural and magnetic properties of both as-sputtered films as well as those made porous using a corrosive electrochemical treatment, as shown in Scheme 1. For a detailed investigation, we focused on two types of samples: high copper content films with an entirely fcc structure and films with a mixed fcc/ bccstructure.

2. EXPERIMENTAL METHODS

2.1. Preparation of Sputtered Films. Thin films were prepared by cosputtering Fe and Cu at room temperature in an AJA International, Inc. magnetron sputtering system. Clean Si substrates (5 × 7 mm2) were mounted and then the chamber was put under vacuum overnight to achieve a pressure ∼1 × 10−7 torr. The Fe was always sputtered at a power of 200 W (direct current, DC)

and the Cu was sputtered at various powers (40, 80, 120, 160, 200, and 240 W, alternating current, AC) for 15 min resulting in thin films with thicknesses between 200 and 300 nm.

2.2. Electrochemical Treatment. The films were treated using an Autolab potentiostat/galvanostat in a 3-electrode configuration. The electrolytic solution was dilute nitric acid in water with acid concentrations ranging from 10 mM to 60 mM. The sputtered films were used at the working electrode with half of the film submerged in the electrolyte. The counter electrode was a platinum wire and the reference electrode was Ag/AgCl (3 M KCl) with 20 mM nitric acid as the exterior solution. All potentials are referred to this electrode. The films were treated at +0.5 V for 60 s. The films were quickly removed from the solution and subsequently rinsed with distilled water and dried. The entire procedure was conducted in air. For characterization, the films were cut using a diamond scribe to remove the half of the film that was not submerged in the electrolyte solution, leaving just the electrochemically treated half.

2.3. Characterization. X-ray diffraction (XRD) patterns were collected on a Philips X'Pert diffractometer using Cu Kα radiation. Field-emission scanning electron microscope (FE-SEM, Zeiss Merlin) with energy-dispersive X-ray spectroscopy (EDX) capabilities was used to characterize the microstructure of the films and the elemental composition. X-ray photoelectron spectroscopy (XPS) analysis was performed using a PHI 5500 multitechnique system (Physical Electronics) with a monochromatic Al Kα source under ultrahigh vacuum. XPS scans were done both on the surface as well as after 15 s of Ar+ sputtering to remove any surface contaminants. The magnetic properties were measured using a MicroSense vibrating sample magnetometer (VSM). The sample magnetization of the VSM data was normalized, in some cases, by mass as determined by inductively coupled plasma (ICP) spectroscopy. The ICP was done on an ICPE 9000 from Shimadzu by dissolving each sample in 3 mL in a 1:1 solution of water and nitric acid (68%).

3. RESULTS AND DISCUSSION

Thin films of Fe_xCu_{1-x} with various compositions were grown using magnetron cosputtering as described above. The elemental composition of the films was determined using EDX and the crystal structure was probed using XRD, as shown in Figure 1a. As expected, the films with the highest Cu content, $Fe_{31}Cu_{69}$ (purple line), were found to have a facecentered cubic (fcc) structure, which is consistent with the native fcc structure of copper. The films with the highest Fe content, $Fe_{73}Cu_{27}$ (black line), were found to have a bodycentered cubic (bcc) structure, consistent with the native structure of iron. Films with the intermediate composition of $Fe_{57}Cu_{43}$ (red line), showed both fcc and bcc peaks indicating that both phases coexist in this case. The magnetic properties of these films were investigated using VSM and the resulting M-H loops are presented in Figure 1b. As expected, the magnetic moment at saturation (MS), remanent magnetization (MR), and coercivity (HC) all increase with increasing Fe content.

Moving forward, we chose to focus on two compositions for electrochemical treatments: the highest Cu content fccfilms (Figure 1, purple lines), and the films showing both fcc and bcc structure (Figure 1, red lines). The films were treated at +0.5 V for 60 s in aqueous solutions of nitric acid with various concentrations (10−60 mM). We also attempted to investigate films that showed only bcc structure (Figure 1, black lines), but were unable to successfully dealloy them. We believe that this was because the films were too Fe-rich and outside of the concentration range suitable for dealloying. For these two samples, we used both XPS and ICP in addition to EDX in order to determine the composition. The ratio of Fe:Cu was determined by all of these techniques and is now indicated in Table 1. As shown, there are differences in compositions as determined by the various techniques which is due to inherent differences in the techniques. For example, XPS is known to only probe the surface and is therefore viewed as indicative of the surface composition only. However, XPS is also the only technique used that can accurately

quantify oxygen content. Furthermore, EDX and XPS are known to have high errors, which is why we conducted ICP. In an effort to be as accurate as possible, we have decided to use the ICP determined composition in referring to the samples from this point forward, and discuss the XPS composition only as it relates to oxygen content.

Figure 2 shows top-view scanning electron microscopy (SEM) images of the high Cu content films (Fe29Cu71) both assputtered (a) and after electrochemical treatment (b−e). The as-sputtered films appear to be composed of fairly round particles and the structure does not seem to be altered by treatment in 10 or 20 mM nitric acid. However, films treated with 40 and 60 mM (d, e) nitric acid are seen to have a distinct porous structure.

The elemental composition and surface oxidation state of the as-sputtered films and porous films (after treatment in 40 mM nitric acid) was determined using XPS as shown in Figure 3. In these experiments, the surface of the films was first etched for 15 s with Ar+ ions in order to remove the outermost layer of atoms and surface contaminants from handling the films in air. We expect that the etching rate is approximately 7 nm/min, so the 15 s of etching should have removed shows only Fe oxides on the surface, but the peak values are shifted to slightly higher binding energies than literature reports for pure Fe which could be due to the formation of an Fe−Cu solid solution. On the other hand, in the spectrum of the porous film the peak positions match those reported for pure Fe and Fe oxides.2,5,20,35 Here, we find a small contribution from Fe0 (blue peaks), and significant contributions from Fe2+ and Fe3+ (purple and green peaks). In the case of the Cu spectra, only Cu0 is found for both the as-sputtered and porous films which is consistent with the fact that Cu is the more noble metal.

The surface composition was determined from XPS and the results are presented in Figure 3. The as-sputtered film is found to have less oxide (17 at %) than the porous film (28 at %). The films were handled and stored in air prior to the XPS measurements, so we expect that a passivation oxidation layer was formed at the film surface, which is why such high oxygen content was determined by XPS. Discounting the oxygen content, the films are found to become more Fe-rich after the electrochemical treatment. The as-sputtered films were found to be Fe25Cu75 (Fe31Cu69 by ICP) while the porous films were found to be Fe78Cu22 (Fe83Cu17 by ICP). As described above, typically in electrochemical dealloying, the more electrochemically active element, in this case iron, should be predominantly removed. However, at high concentrations of the more noble element, above what is referred to as the parting limit, both elements are removed simultaneously. Our results reveal that the relative amount of Cu became lower, which suggests that this composition was above the parting limit.

The structure and magnetic properties of these films were investigated with XRD and VSM, as shown in Figure 4. The XRD diffractograms in Figure 4a show that the films all have an fcc structure and there is no observed change in crystallographic structure as a result of the electrochemical treatment. Despite the increase in Fe content upon dealloying, the fact that the films remain purely fccstructurally is interesting, but consistent with previous reports that the fccstructure can be stabilized in Fe−Cu films up to ∼80% Fe.36 It is worth noting that there are no iron or copper oxide peaks detectable in the XRD patterns, which suggests that the inner parts of the films are metallic, and that the oxide detected by XPS is only present on the surface. In addition, we used high resolution transmission electron microscopy (TEM) and selected area electron diffraction (SAED) to further characterize the crystal structure of the films and have included that data in Figures S2 and S3. In spite of slight oxidation (as revealed by the SAED patterns) is significant that these films contain a large fraction of metallic phases after dealloying (as evidenced by XRD), particularly because there are no noble metals here. Many previous reports have successfully used dealloying to make porous metals with noble metal alloys (Pt, Au, etc.),22,25,26,37,38 but often with nonnoble elements, dealloying causes oxidation.21,27,39,40

The inplane M−H loops for these films are shown in Figure 4b. The films treated at 10 and 20 mM nitric acid have almost identical properties to the as-sputtered films whereas the porous films, those treated with 40 and 60 mM nitric acid, have a higher HC and MS. We note that the loops for the films treated with 40 and 60 mM nitric acid are nosier because those films had less total amount of material and thus lower signal. Because all of the films show the same fcc structure, the changes in magnetic properties could be attributed to either the change in elemental composition and/or the porosity. In this case, we expect that both factors could increase the coercivity. The dealloying process made the films more Fe-rich, which would increase the coercivity and the induced porosity could have the same effect by limiting domain wall propagation. Because both factors could have caused the increase in coercivity, it is difficult to determine the exact cause, although we believe the increased coercivity was due to a combination of these factors. Next, we investigated the effects of the electrochemical treatment on the films showing both fcc and bcc structure (Figure 1, red lines). Figure 5 shows the top-view SEM images of these films both assputtered (a) and after electrochemical treatment (b−d). Similar to the high Cu content films, the films treated with 10 and 20 mM nitric acid (b, c) show little to no change in morphology compared to the as-sputtered films. The films treated with 40 mM nitric acid (d), however, show significant porosity and a loss of the particulate structure. Instead, the occurrence of a 3D network with ligament size of 50−100 nm was evident. Note that films of this composition could not be treated with 60 mM nitric acid without significant delamination/dissolution. Figure 6 shows the results of the XPS analysis for these films and the calculated surface composition. The Fe spectra of the as-sputtered film shows that the surface Fe is entirely oxidized while the surface Fe in the porous film has a significant contribution from Fe0 (blue peaks). For both the assputtered film and the porous film, the Cu is found to be entirely metallic. This is similar to the results for the high Cu content films. The porous film is again more oxidized than the as-sputtered film with 28 at % oxygen compared to 21 at % oxygen in the as-sputtered film. These films, unlike the previous ones, lost Fe during the electrochemical treatment to become more Cu-rich. Disregarding oxygen, the as-sputtered films were found to be Fe64Cu36, whereas the porous film was Fe31Cu69 after etching. These results are consistent with an electrochemical dealloying process below the parting limit.8,23,26,38

Figure 7a shows the XRD diffraction patterns for these films. In the as-sputtered films, the bccpeak is larger than the fccpeak, but after electrochemical treatment the fccpeak increases relative to the bccpeak. This is consistent with the composition change because Cu promotes the fccstructure and, as iron is removed and the films become more Cu-rich, there is larger content of the fccphase present. This points to diffusion of the Cu adatoms during the dealloying treatment.8 Figure 7b shows the in-plane M−H loops for these films. The as-sputtered film (black line) has the highest MS and MR followed by the films treated with 10 and 20 mM nitric acid (blue and green lines). The porous film (red line) is found to have the lowest MS and a slightly higher HC. The reduction in MS is attributed to the change in composition (i.e., reduction in Fe fraction). However, a reduction of Fe content would be expected to decrease the HC, whereas here, the coercivity is increased. Therefore, we attribute the increased coercivity in this case to the induced porosity and the change in crystal structure. Furthermore, this loop has an obvious step in it (i.e., a staircase-like shape), which suggests that there are two distinct contributions to the magnetism. While it is unclear exactly what is causing this step, we believe that the second contribution (with higher coercivity) could be from the newly formed fccphase, in agreement with the XRD data. It is possible that a partially oxidized metal could produce similar data, but in this case, it is unlikely that oxidation is causing the step because XRD in Figure 7a suggests that the films are primarily metallic. Another possible cause of this step is that the dealloying process created porosity through most, but not all, of the film thickness, which was determined by looking at cross sections in SEM (included in Figure S1). It is possible that the two contributions are the porous component and the pristine layer underneath. However, we do not believe this

this the primary cause of the step because the same underlayer is present in the Cu-rich films (also in Figure S1), and in that case, there is no step in the hysteresis loop (Figure 4). It is for these reasons that we believe that the cause of the dual contributions is the presence of both fccand bccphases in these films, whereas in the fcconly films, only a single magnetic contribution is observed. This is consistent with work previously published by our group on FeCu films deposited by electrodeposition which found that films with increased fcc contributions had higher coercivities.41

We further investigated the in-plane and out-of-plane magnetization curves for both as-sputtered films and the porous films (Figure 8). The M−Happlied loops of the high Cu content films (Fe29Cu71) are shown in Figure 8a. Both the assputtered (black lines) and porous (red lines) films were found to be isotropic with very little difference between the in-plane (solid lines) and out-of-plane (dashed lines) loops. However, the films with mixed fccand bccstructure (Fe63Cu37) in Figure 8b were found to be anisotropic. For both the as-sputtered (black lines) and porous (red lines) films MR and HC are all found to be higher in the in-plane direction (solid lines). We believe that this could be due to the Cu rich films being made of magnetic clusters, not necessarily interconnected, so that the in-plane shape anisotropy is not observed. That is, if the magnetic component it primarily made of randomly oriented clusters then we expect the magnetism to be the same in all directions (i.e., no shape anisotropy). Conversely, the ferromagnetic regions in the Fe63Cu37 films are likely to be more abundant and interconnected, which would make them behave more like a typical magnetic thin film than clusters. In this case, we would expect the demagnetizing field to be larger, leading to clear in plane shape anisotropy.

4. CONCLUSIONS

Here we have reported the fabrication of FexCu1−x thin films by cosputtering and the characterization of their magnetic properties. We have also presented a method for creating nanoporosity in these films using a corrosive electrochemical treatment. Remarkably, the fabrication of nanoporous thin films by combining sputter deposition with electrochemical treatments has been largely overlooked in the literature. Hence, this work constitutes one of the first studies on nanoporous magnetic thin films made using these methods. This is of particular interest for use in high-surface-area magnetic components because the induced porosity creates a highsurface-area, whereas the magnetic properties are highly tunable through composition. We found that the microstructure, crystal structure and magnetic properties of these films are all dependent on both initial film composition as well as porosity. Furthermore, the methods developed here can be applied to other systems to create porous magnetic thin films with tunable structural and magnetic properties.

AUTHOR INFORMATION

Corresponding Authors

*E-mail: shaunaaryn.robbennolt@uab.cat (S.R.).

*E-mail: eva.pellicer@uab.cat (E.P.).

*E-mail: jordi.sort@uab.cat (J.S.).

ORCID

Shauna Robbennolt: 0000-0001-5723-7971

Alberto Quintana: 0000-0002-9813-735X

Enric Menendez: 0000-0003-3809-2863

Notes The authors declare no competing financial interest.

ACKNOWLEDGMENTS

This work was supported by the European Research Council under the SPIN-PORICS 2014-Consolidator Grant Agreement 648454, the Spanish Government (MAT2017-86357-C3-1-R, MAT2014-57960-C3-1-R and associated FEDER) and the Generalitat de Catalunya (2017-SGR-292). J.F. acknowledges the Juan de la Cierva Fellowship from MINECO (IJCI-2015- 27030). E.P. is grateful to MINECO for the “Ramon y Cajal” contract (RYC-2012-10839). E.M. acknowledges the European Union’s Horizon 2020 research and innovation programme under the Marie Skłodowska-Curie Grant 665919.

REFERENCES

(1) Wittstock, A.; Zielasek, V.; Biener, J.; Friend, C. M.; Baumer, M.¨ Nanoporous Gold Catalysts for Selective Gas-Phase Oxidative Coupling of Methanol at Low Temperature. Science 2010, 327, 319.

(2) Lozzi, L.; Passacantando, M.; Picozzi, P.; Santucci, S.; den Daas, H. Oxidation of the FeCu(100) Interface. Surf. Sci. 1995, 331, 703− 709.

(3) Zhang, H.; Feng, Y.; Cheng, Y.; Baro, M. D.; Altube, A.; García-´ Lecina, E.; Alcaide, F.; Pellicer, E.; Zhang, T.; Sort, J. Nanoporous FeBased Alloy Prepared by Selective Dissolution: An Effective Fenton Catalyst for Water Remediation. ACS Omega 2017, 2, 653−662.

(4) Miller, A. C.; Simmons, G. W. Copper by XPS. Surf. Sci. Spectra 1993, 2, 55−60.

(5) Biesinger, M. C.; Payne, B. P.; Grosvenor, A. P.; Lau, L. W. M.; Gerson, A. R.; Smart, R. S. C. Resolving Surface Chemical States in XPS Analysis of First Row Transition Metals, Oxides and Hydroxides: Cr, Mn, Fe, Co and Ni. Appl. Surf. Sci. 2011, 257, 2717−2730.

(6) Detsi, E.; Cook, J. B.; Lesel, B. K.; Turner, C. L.; Liang, Y.-L.; Robbennolt, S.; Tolbert, S. H. Mesoporous Ni60Fe30Mn10-Alloy Based Metal/Metal Oxide Composite Thick Films as Highly Active and Robust Oxygen Evolution Catalysts. Energy Environ. Sci. 2016, 9, 540− 549.

(7) Parmigiani, F.; Pacchioni, G.; Illas, F.; Bagus, P. S. Studies of the Cu-O Bond in Cupric Oxide by X-Ray Photoelectron Spectroscopy and Ab Initio Electronic Structure Models. J. Electron Spectrosc. Relat. Phenom. 1992, 59, 255−269.

(8) Erlebacher, J.; Aziz, M. J.; Karma, A.; Dimitrov, N.; Sieradzki, K. Evolution of Nanoporosity in Dealloying. Nature 2001, 410, 450−453.

(9) Kibsgaard, J.; Jackson, A.; Jaramillo, T. F. Mesoporous Platinum Nickel Thin Films with Double Gyroid Morphology for the Oxygen Reduction Reaction. Nano Energy 2016, 29, 243−248.

(10) Zhang, J.; Li, C. M. Nanoporous Metals: Fabrication Strategies and Advanced Electrochemical Applications in Catalysis, Sensing and Energy Systems. Chem. Soc. Rev. 2012, 41, 7016−7031.

(11) Cook, J. B.; Kim, H.-S.; Lin, T. C.; Robbennolt, S.; Detsi, E.; Dunn, B. S.; Tolbert, S. H. Tuning Porosity and Surface Area in Mesoporous Silicon for Application in Li-Ion Battery Electrodes. ACS Appl. Mater. Interfaces 2017, 9, 19063−19073.

(12) Lang, X.; Hirata, A.; Fujita, T.; Chen, M. Nanoporous Metal/ Oxide Hybrid Electrodes for Electrochemical Supercapacitors. Nat. Nanotechnol. 2011, 6, 232−236.

(13) Hu, Y.-S.; Guo, Y.-G.; Sigle, W.; Hore, S.; Balaya, P.; Maier, J. Electrochemical Lithiation Synthesis of Nanoporous Materials with Superior Catalytic and Capacitive Activity. Nat. Mater. 2006, 5, 713− 717.

(14) Rauda, I. E.; Buonsanti, R.; Saldarriaga-Lopez, L. C.; Benjauthrit, K.; Schelhas, L. T.; Stefik, M.; Augustyn, V.; Ko, J.; Dunn, B.; Wiesner, U.; Milliron, D. J.; Tolbert, S. H. General Method for the Synthesis of Hierarchical Nanocrystal-Based Mesoporous Materials. ACS Nano 2012, 6, 6386−6399.

(15) Thomas, A.; Goettmann, F.; Antonietti, M. Hard Templates for Soft Materials: Creating Nanostructured Organic Materials. Chem. Mater. 2008, 20, 738−755.

(16) Yang, P.; Zhao, D.; Margolese, D. I.; Chmelka, B. F.; Stucky, G. D. Block Copolymer Templating Syntheses of Mesoporous Metal Oxides with Large Ordering Lengths and Semicrystalline Framework. Chem. Mater. 1999, 11, 2813−2826.

(17) Fan, J.; Zhang, J.; Solsona, P.; Surinach, S.; Baro, M. D.; Sort, J.; Pellicer, E. Nanocasting Synthesis of Mesoporous SnO2 with a Tunable Ferromagnetic Response through Ni Loading. RSC Adv. 2016, 6, 104799−104807.

(18) Hsueh, H.-Y.; Yao, C.-T.; Ho, R.-M. Well-Ordered Nanohybrids and Nanoporous Materials from Gyroid Block Copolymer Templates. Chem. Soc. Rev. 2015, 44, 1974−2018.

(19) Bolton, J.; Bailey, T. S.; Rzayev, J. Large Pore Size Nanoporous Materials from the Self-Assembly of Asymmetric Bottlebrush Block Copolymers. Nano Lett. 2011, 11, 998−1001.

(20) den Daas, H.; Passacantando, M.; Lozzi, L.; Santucci, S.; Picozzi P. The Interaction of Cu(100)-Fe Surfaces with Oxygen Studied by XRay Photoelectron Spectroscopy. Surf. Sci. 1994, 317, 295−302.

(21) Qiu, H. J.; Peng, L.; Li, X.; Xu, H. T.; Wang, Y. Using Corrosion to Fabricate Various Nanoporous Metal Structures. Corros. Sci. 2015, 92, 16−31.

(22) Jin, H.-J.; Weissmüller, J. Bulk Nanoporous Metal for Actuation. Adv. Eng. Mater. 2010, 12, 714−723.

(23) Tappan, B. C.; Steiner, S. A.; Luther, E. P. Nanoporous Metal Foams. Angew. Chem., Int. Ed. 2010, 49, 4544−4565.

(24) Sun, L.; Chien, C.-L.; Searson, P. C. Fabrication of Nanoporous Nickel by Electrochemical Dealloying. Chem. Mater. 2004, 16, 3125− 3129.

(25) Simmonds, M. C.; Kheyrandish, H.; Colligon, J. S.; Hitchman, M. L.; Cade, N.; Iredale, J. The Observation of a Threshold in the DeAlloying of Sputter-Deposited PtxAl1−x Alloy Thin Films. Corros. Sci. 1998, 40, 43−48.

(26) McCue, I.; Benn, E.; Gaskey, B.; Erlebacher, J. Dealloying and Dealloyed Materials. Annu. Rev. Mater. Res. 2016, 46, 263−286.

(27) Peecher, B. E.; Hampton, J. R. Dealloying Behavior of NiCo and NiCoCu Thin Films. Int. J. Electrochem. 2016, 2016, 1−10.

(28) Thorp, J. C.; Sieradzki, K.; Tang, L.; Crozier, P. A.; Misra, A.; Nastasi, M.; Mitlin, D.; Picraux, S. T. Formation of Nanoporous Noble Metal Thin Films by Electrochemical Dealloying of PtxSi1−x. Appl. Phys. Lett. 2006, 88, 033110.

(29) Okman, O.; Lee, D.; Kysar, J. W. Fabrication of Crack-Free Nanoporous Gold Blanket Thin Films by Potentiostatic Dealloying. Scr. Mater. 2010, 63, 1005−1008.

(30) Robbie, K.; Friedrich, L. J.; Dew, S. K.; Smy, T.; Brett, M. J. Fabrication of Thin Films with Highly Porous Microstructures. J. Vac. Sci. Technol., A 1995, 13, 1032−1035.

(31) Alvarez, R.; García-Martín, J. M.; Macías-Montero, M.; Gonzalez-Garcia, L.; Gonzalez, J. C.; Rico, V.; Perlich, J.; Cotrino, J.; Gonzalez-Elipe, A. R.; Palmero, A. Growth Regimes of Porous Gold Thin Films Deposited by Magnetron Sputtering at Oblique Incidence: From Compact to Columnar Microstructures. Nanotechnology 2013, 24, 045604.

(32) Kuch, W.; Salvietti, M.; Gao, X.; Lin, M. T.; Klaua, M.; Barthel, J.; Mohan, C. V.; Kirschner, J. Artificially Ordered FeCu Alloy Superlattices on Cu(001). ii. Spin-Resolved Electronic Properties and Magnetic Dichroism. Phys. Rev. B: Condens. Matter Mater. Phys. 1998, 58, 8556−8565.

(33) Castin, N.; Messina, L.; Domain, C.; Pasianot, R. C.; Olsson, P. Improved Atomistic Monte Carlo Models Based on Ab-Initio-Trained Neural Networks: Application to FeCu and FeCr Alloys. Phys. Rev. B: Condens. Matter Mater. Phys. 2017, 95, 214117.

(34) Vaks, V. G.; Khromov, K. Y.; Pankratov, I. R.; Popov, V. V. Statistical Theory of Diffusion in Concentrated bcc and fcc Alloys and Concentration Dependencies of Diffusion Coefficients in bcc Alloys FeCu, FeMn, FeNi, and FeCr. J. Exp. Theor. Phys. 2016, 123, 59−85.

(35) Tan, B. J.; Klabunde, K. J.; Sherwood, P. M. A. X-Ray Photoelectron Spectroscopy Studies of Solvated Metal Atom Dispersed Catalysts. Monometallic Iron and Bimetallic Iron-Cobalt Particles on Alumina. Chem. Mater. 1990, 2, 186−191.

(36) Huang, J. Y.; Jiang, J. Z.; Yasuda, H.; Mori, H. Phys. Rev. B: Condens. Matter Mater. Phys. 1998, 58, R11817−R11820.

(37) Rö sner, H.; Parida, S.; Kramer, D.; Volkert, C. A.; Weissmüller, J. Reconstructing a Nanoporous Metal in Three Dimensions: An Electron Tomography Study of Dealloyed Gold Leaf. Adv. Eng. Mater. 2007, 9, 535−541.

(38) Gao, P.; Zhu, Z.; Ye, X.; Wu, Y.; Jin, H.; Volinsky, A. A.; Qiao, L.; Su, Y. Defects Evolution in Nanoporous Au(Pt) During Dealloying. Scr. Mater. 2016, 113, 68−70.

(39) Qi, Z.; Gong, Y.; Zhang, C.; Xu, J.; Wang, X.; Zhao, C.; Ji, H.; Zhang, Z. Fabrication and Characterization of Magnetic Nanoporous Cu/(Fe,Cu)3O4 Composites with Excellent Electrical Conductivity by One-Step Dealloying. J. Mater. Chem. 2011, 21, 9716−9724.

(40) Park, B. J.; Chen, Y. M.; Ohkubo, T. Metallic Porous Materials' Design with Phase Separation in Fe-Cu and Co-Cu Systems. Intermetallics 2009, 17, 958−961.

(41) Dislaki, E.; Sort, J.; Pellicer, E. Parametric Aqueous Electrodeposition Study and Characterization of Fe−Cu Films. Electrochim. Acta 2017, 231, 739−748.

FIGURES

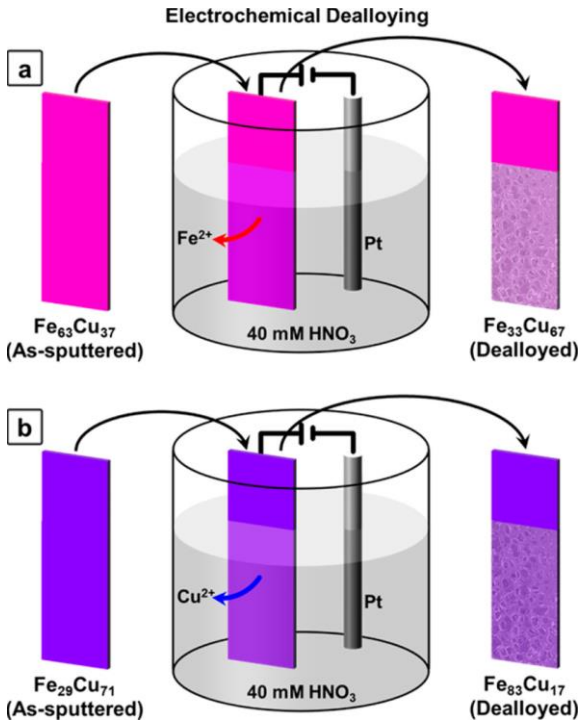

Scheme 1. Cartoon Representing the Electrochemical Dealloying Step Using the 40 mM HNO_3 Solution, against a Pt Reference Electrode: (a) High-Fe Film Predominantly Loses Fe, Becoming More Cu-Rich ; (b) High-Cu Films Predominantly Lose Cu, Becoming More Fe-Rich.

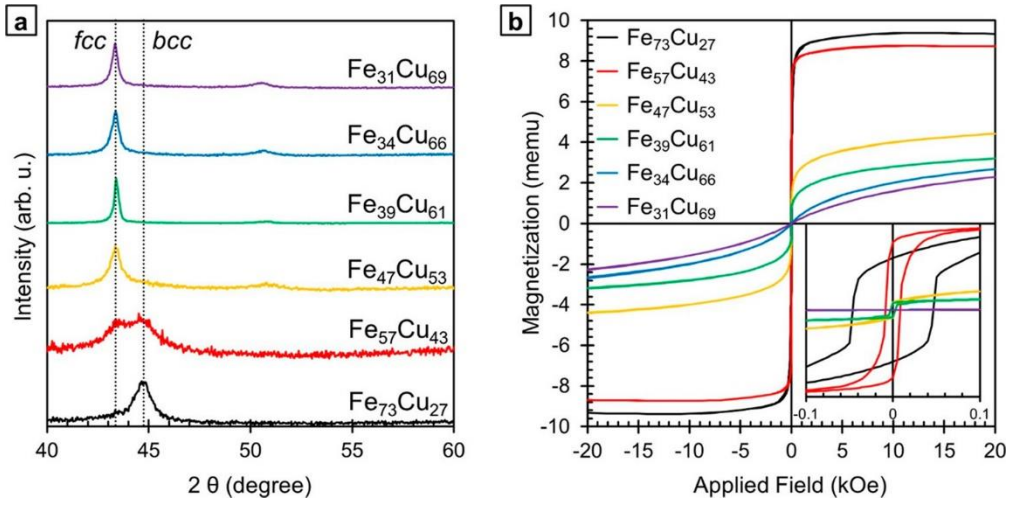

Figure 1. (a) XRD diffraction patterns of as-sputtered films of various compositions (as determined by EDX analysis). (b) In-plane magnetic hysteresis loops of as-sputtered films of various compositions. Inset shows the loops zoomed into the low applied field region. Note that for these samples, the sample size was kept constant, so that the magnetic moment values can be compared even if they are not normalized by volume or mass.

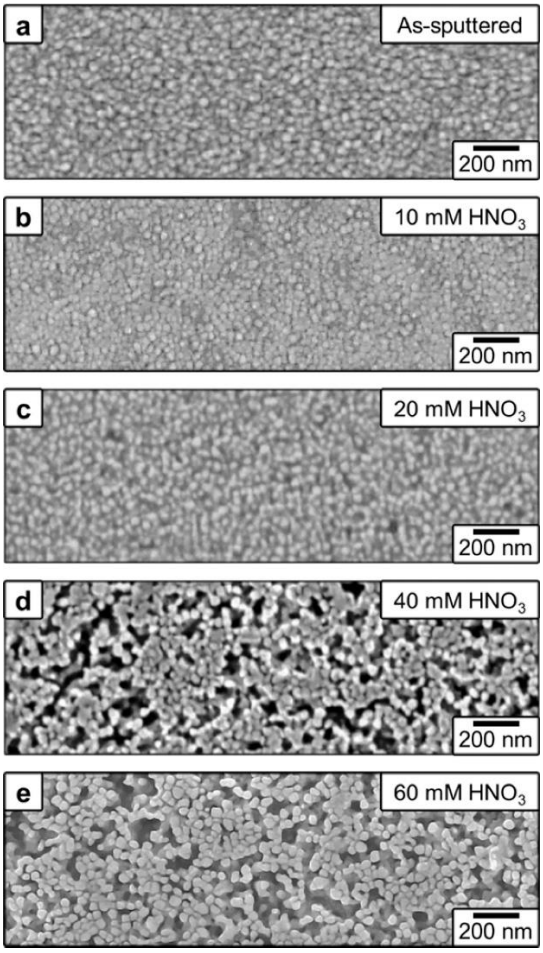

Figure 2. Top-view SEM micrographs of $Fe_{29}Cu_{71}$ films (a) as-sputtered and after treatment for 60 s at +0.5 V in (b) 10 mM HNO_3, (c) 20 mM HNO_3, (d) 40 mM HNO_3, and (e) 60 mM HNO_3.

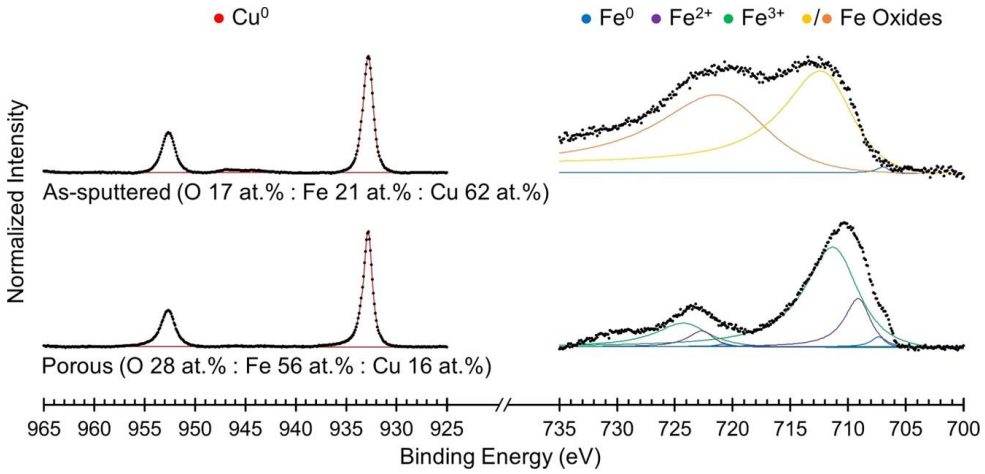

Figure 3. Cu and Fe XPS spectra of high-Cu-content films with fits. Measurements were taken after 15 s of Ar^+ etching to remove surface contaminants. Black dots correspond to raw data points, whereas colored lines are fitted peaks color coded to correspond to oxidation state. Different oxidation states were assigned according to literature reports found using the NIST XPS database.(2,4,7,20,35)

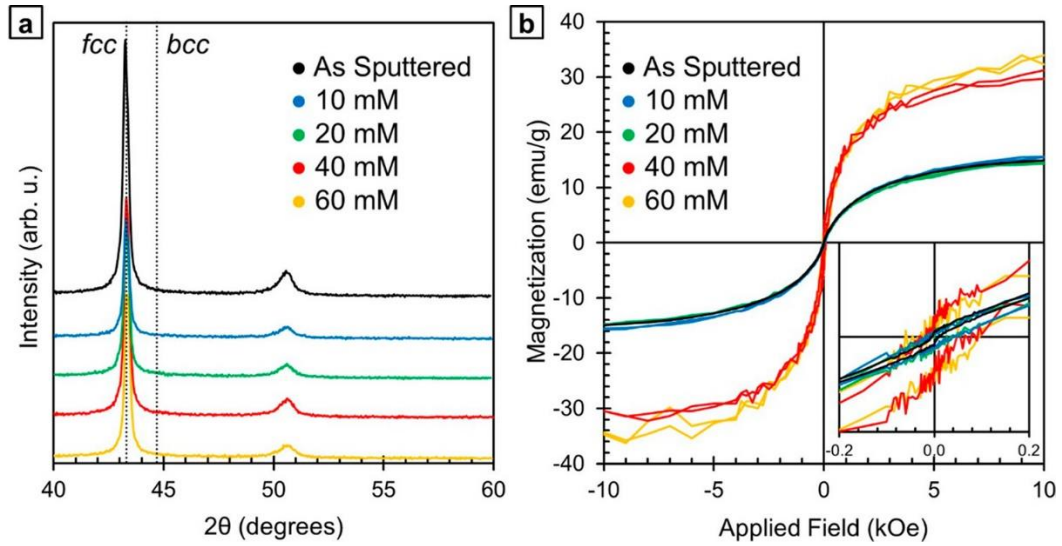

Figure 4. (a) XRD diffractograms of $Fe_{29}Cu_{71}$ films both as-sputtered (black) and after treatment at +0.5 V for 60 s in various concentrations of nitric acid (10 mM, blue line; 20 mM, green line; 40 mM, red line; 60 mM, yellow line). (b) In-plane magnetic hysteresis loops of the same films. Inset shows the loops zoomed into the low-applied-field region.

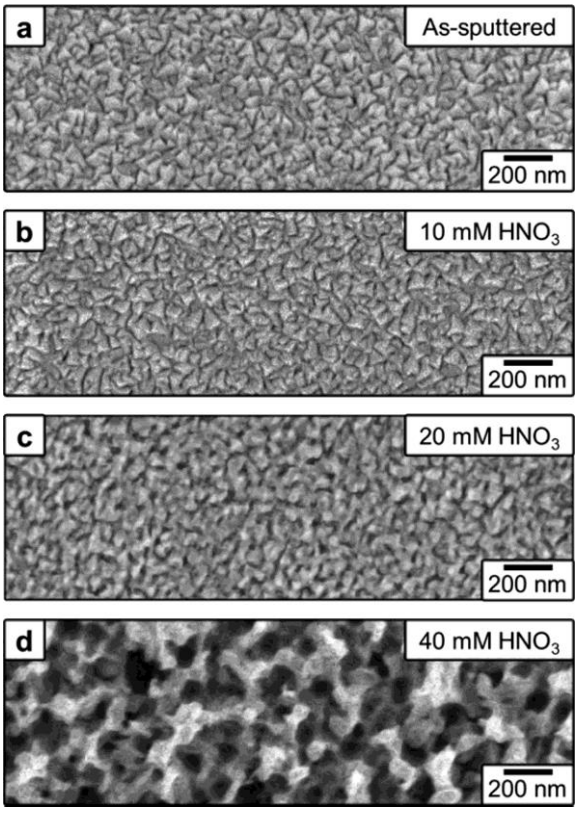

Figure 5. Top-view SEM micrographs of $Fe_{63}Cu_{37}$ films (a) as-sputtered and after treatment for 60 s at +0.5 V in (b) 10 mM HNO_3, (c) 20 mM HNO_3, and (d) 40 mM HNO_3.

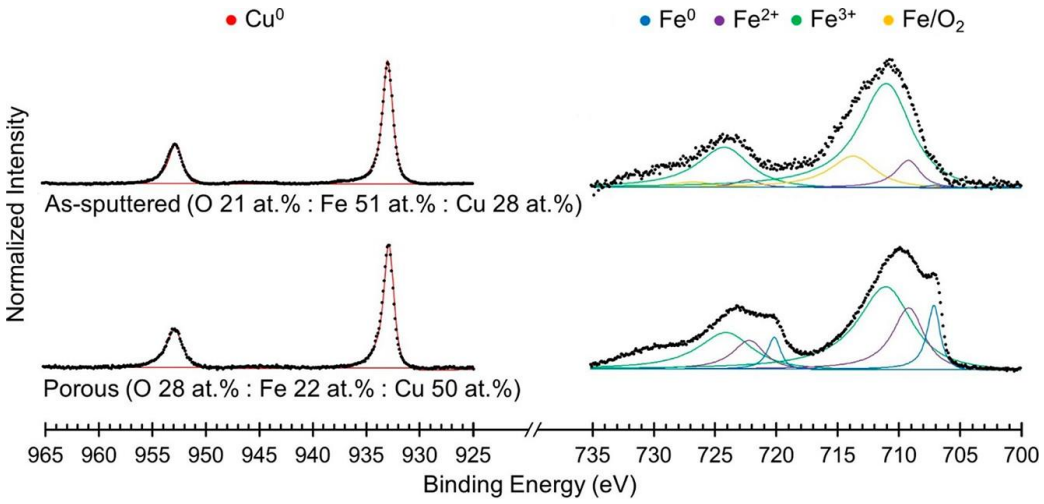

Figure 6. Cu and Fe XPS spectra of high-Fe-content films with fits. Measurements were taken after 15 s of Ar^+ etching to remove surface contaminants. Black dots correspond to raw data points, whereas colored lines are fitted peaks color coded to correspond to oxidation state. Different oxidation states were assigned according to literature reports found using the NIST XPS database.(2,5,8,20,35)

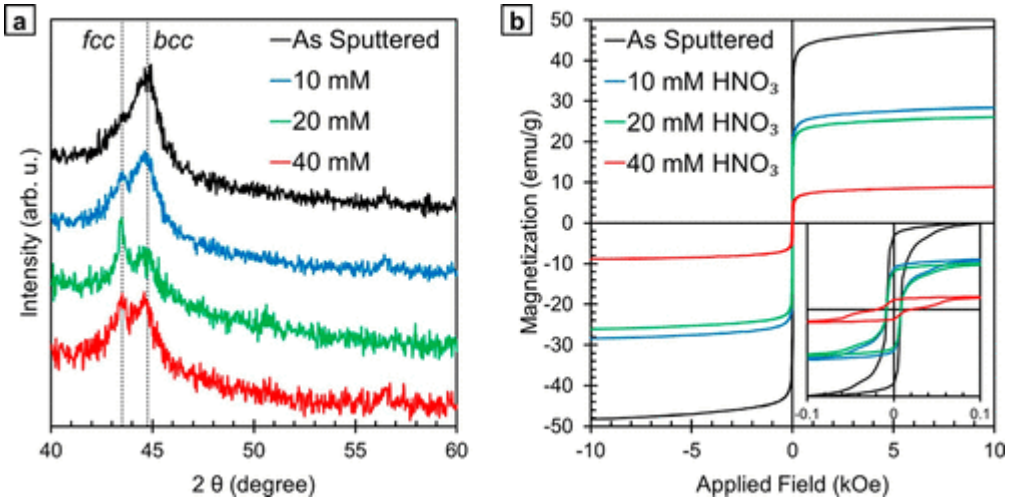

Figure 7. (a) XRD diffractograms of $Fe_{63}Cu_{37}$ films both as-sputtered (black) and after treatment at +0.5 V for 60 s in various concentrations of nitric acid (10 mM, blue line; 20 mM, green line; 40 mM, red line). (b) In-plane magnetic hysteresis loops of the same films. Inset shows the loops zoomed into the low-applied-field region.

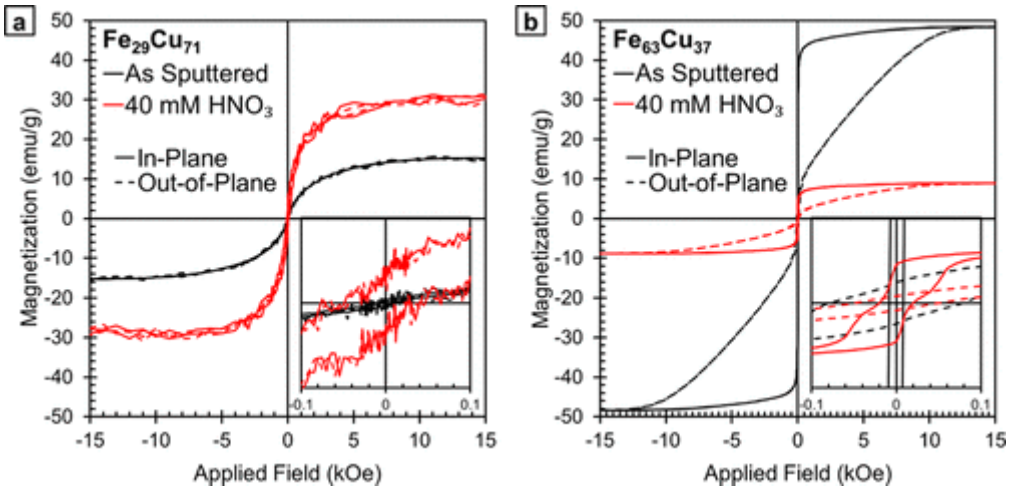

Figure 8. In-plane (solid lines) and out-of-plane (dashed lines) magnetic hysteresis loops of (a) $Fe_{29}Cu_{71}$ films and (b) $Fe_{63}Cu_{37}$ films both as-sputtered (black) and porous (red). Insets show the loops zoomed into the low-applied-field region.

TABLES

Table 1. Sample Composition Data, Acquired Using EDX, XPS, and ICP.

	as-sputtered						dealloyed			
	EDX		XPS		ICP		XPS		ICP	
sample	Fe	Cu	Fe	Cu	Fe	Cu	Fe	Cu	Fe	Cu
1	31	69	25	75	29	71	78	22	83	17
2	34	66								
3	39	61								
4	47	53								
5	57	43	64	36	63	37	31	69	33	67
6	73	27								